Available online at www.sciencedirect.com
ScienceDirect
International Journal of Mass Spectrometry 257 (2006) 34–40
International Journal of Mass Spectrometry
www.elsevier.com/locate/ijms

Kinetics of electron impact ionization and ion-molecule reactions of pyridine

C.Q. Jiao [a], C.A. DeJoseph Jr. [b], R. Lee [b], A. Garscadden [b,*]

[a] *Innovative Scientific Solutions Inc., Dayton, OH 45440-3638, USA*
[b] *Air Force Research Laboratory, Wright-Patterson AFB, OH 45433-7251, USA*

Received 21 December 2005; received in revised form 14 June 2006; accepted 14 June 2006
Available online 18 July 2006

Abstract

Dissociative ionization of pyridine by electron impact is investigated using Fourier transform mass spectrometry (FTMS). Absolute total and partial ionization cross-sections are measured as functions of electron energy in the range of 10–200 eV. The parent ion and 15 fragment ions are observed, with the total cross-section reaching a maximum of 1.5×10^{-15} cm^2 at ∼90 eV. Four important ions generated at 50 eV electron energy, $C_5H_5N^+$, $C_4H_4^+$, $C_4H_3^+$, and $C_4H_2^+$, are found to react with pyridine via mechanisms of charge transfer and proton transfer. $C_4H_4^+$ also undergoes condensation with pyridine followed by H elimination.
Published by Elsevier B.V.

Keywords: Ionization; Pyridine; Ion-molecule; Cross-section

1. Introduction

The dissociative ionization of pyridine has been one of the topics of debate for decades in the area of mass spectrometry, especially with regard to the isomer composition of the product ion $C_4H_4^+$, the fragmentation mechanism, and the appearance energies of the product ions [1–11]. The reactions of ions generated from the ionization, including collision-induced dissociation (CID), have been studied [4,5,7]. In this paper we report the results of our recent measurement on absolute dissociative ionization cross-sections of pyridine by electron impact. Results of some gas phase ion-molecule reactions in pyridine will also be presented. This study was initiated by the need for comparison of experimental data with a theoretical study by Huo and co-workers, who have recently performed calculations on the ionization cross-sections of benzene and pyridine, as part of a program to investigate the role played by electron impact dissociative ionization in the processes of DNA damage by space radiation [12].

2. Experimental

All of the experiments were performed using a modified Extrel FTMS equipped with a cubic ion cyclotron resonance trapping cell (5 cm on a side) and a 2 T superconducting magnet [13]. The theory and methodology of FTMS have been well documented in the literature [14–16]. Pyridine (99.9+%, Aldrich) or pyridine-d_5 (100.0 at.% D, Aldrich) was further processed by applying multiple liquid N_2 freeze-pump-thaw cycles to remove non-condensable gases. For the ionization cross-section measurements, pyridine was mixed with Ar (99.999%, Matheson) in a ratio of about 1:1 to a total pressure of ∼15 Torr, as determined by capacitance manometry. The mixture was then admitted through a precision leak valve (Varian controlled leak valve) into the FTMS system. Ions are formed by electron impact in the trapping cell at pressures in the 10^{-7} Torr range. An electron gun (Kimball Physics ELG2, Wilton, NH) irradiates the cell with a few hundred picocoulombs of low-energy electrons (detailed description of the electron beam is given below). The motion of the ions is constrained radially by the superconducting magnetic field and axially by an electrostatic potential (trapping potential) applied to the trap faces that are perpendicular to the magnetic field. The trapping potential is usually set to 10 V (see below for more details about the potential profile in the trapping cell). Ions of all mass-to-charge ratios are simultaneously

* Corresponding author. Tel.: +1 937 2552246; fax: +1 937 6564657.
E-mail address: alan.garscadden@wpafb.af.mil (A. Garscadden).

1387-3806/$ – see front matter. Published by Elsevier B.V.
doi:10.1016/j.ijms.2006.06.007

and coherently excited into cyclotron orbits using stored waveform inverse Fourier transform (SWIFT) [17–19] applied to two opposing trap faces which are parallel to the magnetic field. Following cyclotron excitation, the image currents induced on the two remaining faces of the trap are amplified, digitized and Fourier analyzed to yield a mass spectrum.

FTMS is an established technique for studying the kinetics of charged particle reactions, in which the ion peak heights are used to evaluate the number of ions in the cell [20]. In this study, the intensity ratios of the ions from pyridine to Ar^+ give cross-sections relative to those for electron impact ionization of Ar [21], since the pressure ratio of pyridine to Ar is known. The pressure ratio of pyridine to Ar in the trapping cell region is equal to the pressure ratio in the manifold, based on the following reasoning. Given the pressures in the manifold and the trapping cell region, the leak valve opening, i.e., the gap between the sapphire and the metal gasket, is estimated to be on the order of submicron. The gap is therefore smaller than the mean free path of atoms/molecules in the manifold, which is on the order of a micron, and therefore diffusion of the gas through the leak valve is characterized by molecular flow, which is proportional to $P_m M^{-0.5}$, where P_m is the manifold pressure and M is the species atomic/molecular mass. At the low pressures in the trapping cell region, flow to the cryopump (1500 l/s) is likewise molecular with a conductance of approximately 65 l/s through the connecting vacuum lines. Therefore the pump rate out of the trapping cell is proportional to $P_t M^{-0.5}$, where P_t is the pressure in the trapping cell. In summary, at equilibrium P_t depends on P_m and the leak valve aperture but not M because both inflow and out-flow are diffusive and the atomic/molecular mass effect is cancelled out. The absence of mass discrimination in the pressure ratio of the trapping cell region is confirmed by experiments in which a mixture of Ar and Xe gases is used and the measured ion intensity ratio is compared to the known ionization cross-sections of these gases in literature [22]. A typical experiment is finished during a timeframe in which there is no significant pressure change in the manifold so that the pressure ratio is constant.

To study the subsequent reactions of ions generated from electron impact ionization with their parent molecule, a mixture of pyridine and Ar with a ratio of ~1:20 was used. The ion to be studied is selected by using SWIFT to eject other ions out of the trapping cell, followed by a cooling period in which the ion undergoes multiple collisions with Ar at a total pressure of $\sim 1 \times 10^{-5}$ Torr for various times, typically 500 ms. SWIFT is used again to select the ion to be studied from others that are formed during the cooling period, followed by a programmed reaction time varying from 0 to 1000 ms. The cooling period can serve two purposes: (1) excited ions are thermalized by collisions with Ar atoms, and/or (2) excited ions with reaction rates greater than the ground state ions are exhausted. The pressure of Ar and the length of the cooling period are adjusted so that at the end of the cooling period there are still sufficient reactant ions to study and their reaction shows a single exponential decay to the end of the reaction time at which only a few percent of the reactant ions are left over. With the large Ar partial pressure, Ar^+ is overpopulated during electron impact ionization, resulting in a significant space charge effect. To eliminate this effect, a single frequency rf waveform is applied during the electron beam event to continuously eject Ar^+ out of the trapping cell.

The trapping cell of the Extrel FTMS was modified by adding a pair of screen electrodes in front of the trapping plates. A significant improvement to the quality of the cross-section data has been achieved by this modification: holding the screens at ground potential produces the particle-in-a-box potential (rather than the harmonic oscillator potential) along the z-axis of the trapping cell [23]. Thus, it is possible to apply relatively high potentials to trap more kinetically energetic ions while in most of the volume of the cell the potential drop is small enough to avoid the broadening of the electron energy distribution. Wang and Marshall have given a detailed description of the design of the screen electrodes [24]. When the trapping potential is set to 10 V as mentioned above, the potential drop within the screen electrode region along the z-axis is estimated to be 0.3 V.

The Kimball Physics ELG-2 electron gun is rated for energies of 10–1000 eV with beam currents of 1 nA to 3 μA. The energy spread of the beam is about 0.25 eV plus the space charge well of the beam [25]. Combining the electron energy spread in the electron source and the potential drop in the trapping cell mentioned above, we estimate the uncertainty of the ionizing electron energies in the FTMS trapping cell to be ±0.6 eV.

3. Results and discussion

Electron impact ionization of pyridine generates the parent ion and 15 fragment ions with cross-sections greater than 10^{-18} cm^2 at 30 eV. Fig. 1 shows the total cross-section and partial cross-sections for these ions as functions of electron energy in the range of 10–200 eV. The ions listed in Fig. 1 are identified among the possible isobar ions by accurate mass determination in a high mass-resolution spectrum and by comparing mass spectra of pyridine and pridine-d_5. In theory, pyridine can have two possible isobar ions at some observed masses, for example, $C_4H_4^+$ and $C_3H_2N^+$ at m/z 52. However, we find that at most of the masses only one isobar ion is present, the other one being absent or negligibly small. The m/z 27 and 38 are exceptions, with both isobar ions, as listed in Fig. 1, having comparable intensities. The parent ion $C_5H_5N^+$ is the most abundant ion throughout the energy range, and its branching ratio drops quickly from near 100% at its threshold to approximately 30% at 50 eV, where it remains approximately level to 200 eV. The most abundant fragment ion throughout the energy range is $C_4H_4^+$, which together with $C_5H_5N^+$ contribute approximately 55% or more of the ion population at all energies studied. Fig. 2 shows a comparison between our measured total ionization cross-section and the calculations of Huo and co-workers [12]. Also shown are error bars which represent the ±18% uncertainty in our absolute data. As can be seen, within the uncertainty of our experiment, there is good agreement over the energy range of our measurements. In general, the FTMS determined total cross-section is greater than the calculated cross-section, and displays a broader peak in the energy dependence profile, with a maximum of 1.5×10^{-15} cm^2 at ~90 eV.

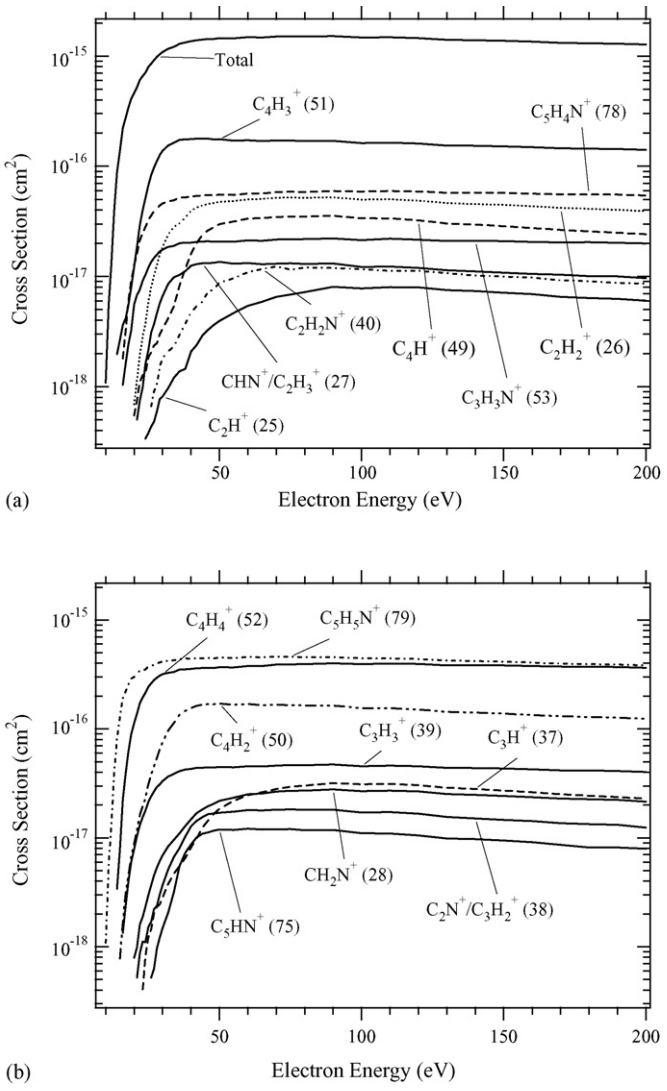

Fig. 1. Absolute cross-sections for electron impact ionization on pyridine. For visual clarity data are presented in plots (a) and (b), in which scales are set to the same for easy comparison of the amplitudes for different ionization channels. The numbers in parentheses in the labels are the nominal masses of the ions. The contributions from the isobar ions, C_2N^+ and $C_3H_2^+$ at *m/z* 38, CHN^+ and $C_2H_3^+$ at *m/z* 27, are not resolved. Combined with the uncertainty in the standard cross-section of Ar for calibration, the estimated uncertainty of the cross-section data is ±18%.

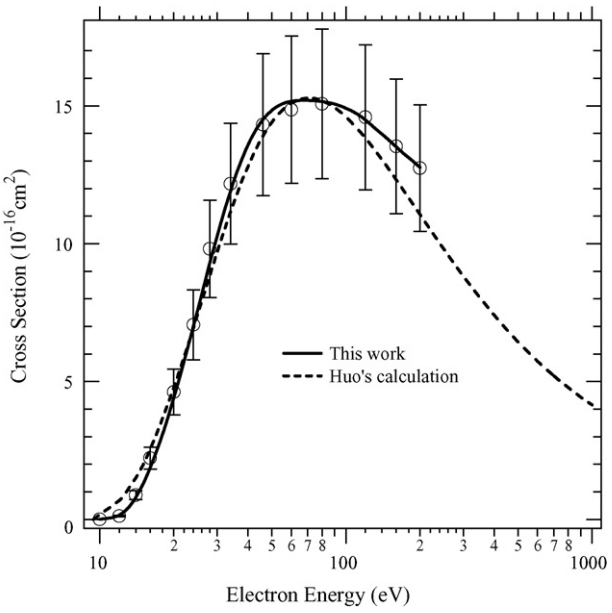

Fig. 2. Comparison between the measured total ionization cross-section in this work and the calculations of Huo and co-workers [12]. Error bars indicate ±18% uncertainty in our measurements. The agreement is very good. Only every third measured data point is plotted for clarity. There was no normalization of the experimental and theoretical results.

At energies below 20 eV, the dominant ions are $C_5H_5N^+$, $C_4H_4^+$, $C_4H_3^+$, $C_4H_2^+$, $C_5H_4N^+$, $C_3H_3^+$, and $C_3H_3N^+$. The cross-sections for these seven species are listed in Table 1 over the full energy range of the experiment. Information on the neutral product partners in forming these fragment ions can be obtained from the following overview of the possible fragmentation pathways. From three studies of metastable ions by Dickinson et al. [1] by Lifshitz et al. [5] and by Arakawa and Yoshikawa [10] one can summarize that the parent ion $C_5H_5N^+$ fragments forming $C_4H_4^+ + HCN$ and $C_5H_4N^+ + H$; $C_4H_4^+$ in turn undergoes further dissociation to form $C_4H_3^+ + H$ and $C_4H_2^+ + H_2$, and $C_5H_4N^+$ dissociates to form $C_4H_3^+ + HCN$. The dissociation products from $C_4H_4^+$ are also confirmed by the collision-induced dissociation experiments in the Lifshitz et al.'s study [5]. In a study on the benzene ion fragmentation by Baer et al., $C_3H_3^+$ and $C_4H_4^+$ were found to be formed, in competition with one another, from a common structure of the benzene ion, with the ratio of $C_3H_3^+$ and $C_4H_4^+$ intensities increasing with the internal energy. This is in accordance with predictions of RRKM theory, within a range of low energies [26]. The pathway forming $C_3H_3^+$ from the pyridine ion has not been reported. If we assume a similar fragmentation pathway of $C_5H_5N^+$ forming $C_3H_3^+ + C_2H_2N$ and $C_4H_4^+ + HCN$ in a competing manner, one should expect the ratio of $C_3H_3^+$ and $C_4H_4^+$ intensities to also increase with the electron energy, because the formation of $C_3H_3^+$ involves only bond cleavage while the formation of $C_4H_4^+$ involves an additional rearrangement, and thus has a relatively low activation energy and small frequency factor [27]. Indeed the plot of the $C_3H_3^+/C_4H_4^+$ ratio shown in Fig. 3 displays this type of behavior at low energies. Data at high energies in Fig. 3 may not be very informative because the contribution of successive decompositions increases resulting in a rather complex matrix of fragmentation paths. Fig. 3 also shows the branching ratio of $C_4H_3^+$ as a function of electron energy, which shows a sudden increases at ~17 eV, probably reflecting the fact that two precursors contribute to the formation of $C_4H_3^+$ as mentioned above: near threshold energies, $C_4H_3^+$ is formed by the $C_4H_4^+$ fragmentation, and after the onset of $C_5H_4N^+$ at 16 eV, it is also formed by the $C_5H_4N^+$ fragmentation. It is not possible to define the neutral products from the formation of $C_3H_3N^+$.

The ion-molecule reactions in pyridine have been studied for the four most abundant ions formed by electron impact at 50 eV, $C_5H_5N^+$, $C_4H_4^+$, $C_4H_3^+$, and $C_4H_2^+$. Each ion to be studied is first isolated from other ionization product ions and then allowed to thermalize by multiple collisions with Ar gas prior to their

Table 1
Absolute partial cross-sections in units of 10^{-16} cm^2, for electron impact ionization of pyridine for the production of the seven most significant ions observed at low energies (i.e., below 20 eV)

Energy (eV)	$C_3H_3^+$	$C_4H_2^+$	$C_4H_3^+$	$C_4H_4^+$	$C_3H_3N^+$	$C_5H_4N^+$	$C_5H_5N^+$	Total
10							0.01	0.01
11							0.05	0.05
12							0.13	0.13
13							0.39	0.39
14			0.02	0.03			0.83	0.88
15		0.01	0.03	0.08			1.3	1.4
16	0.01	0.02	0.04	0.22	0.01	0.02	1.9	2.2
17	0.02	0.03	0.04	0.39	0.02	0.03	2.2	2.8
18	0.04	0.05	0.05	0.61	0.02	0.06	2.6	3.4
19	0.06	0.07	0.08	0.89	0.03	0.09	2.9	4.1
20	0.08	0.09	0.12	1.1	0.06	0.13	3.0	4.6
21	0.10	0.12	0.19	1.4	0.07	0.16	3.2	5.2
22	0.13	0.16	0.29	1.7	0.08	0.21	3.4	6.1
23	0.15	0.19	0.40	2.0	0.09	0.25	3.5	6.6
24	0.18	0.23	0.51	2.1	0.10	0.28	3.5	7.1
25	0.21	0.31	0.67	2.4	0.12	0.32	3.7	8.0
26	0.24	0.38	0.83	2.6	0.14	0.36	3.8	8.6
27	0.27	0.46	0.98	2.8	0.15	0.39	3.9	9.2
28	0.29	0.54	1.1	3.0	0.16	0.42	4.0	9.8
29	0.31	0.65	1.3	3.1	0.17	0.44	4.1	10
30	0.33	0.75	1.4	3.2	0.18	0.46	4.2	11
32	0.37	0.97	1.5	3.3	0.19	0.48	4.2	12
34	0.39	1.1	1.6	3.3	0.19	0.49	4.3	12
36	0.41	1.4	1.7	3.5	0.20	0.52	4.4	13
38	0.42	1.5	1.7	3.5	0.20	0.52	4.4	13
40	0.43	1.6	1.8	3.6	0.20	0.53	4.4	14
42	0.44	1.6	1.8	3.6	0.21	0.54	4.5	14
44	0.44	1.7	1.8	3.6	0.21	0.54	4.5	14
46	0.44	1.7	1.8	3.6	0.21	0.55	4.5	14
48	0.44	1.7	1.8	3.6	0.21	0.54	4.4	14
50	0.45	1.7	1.8	3.7	0.21	0.55	4.5	15
55	0.44	1.7	1.7	3.7	0.21	0.55	4.5	14
60	0.45	1.7	1.7	3.8	0.21	0.57	4.6	15
65	0.45	1.7	1.7	3.8	0.21	0.57	4.5	15
70	0.46	1.7	1.7	3.9	0.22	0.58	4.6	15
75	0.47	1.7	1.7	3.9	0.22	0.59	4.6	15
80	0.46	1.6	1.7	3.9	0.22	0.58	4.6	15
90	0.47	1.6	1.7	4.0	0.22	0.60	4.6	15
100	0.45	1.6	1.6	3.9	0.21	0.59	4.5	15
110	0.46	1.6	1.6	4.0	0.22	0.60	4.4	15
120	0.45	1.5	1.6	3.9	0.22	0.59	4.4	15
130	0.44	1.4	1.5	3.8	0.21	0.57	4.2	14
140	0.44	1.4	1.5	3.8	0.21	0.58	4.2	14
150	0.43	1.4	1.5	3.8	0.21	0.57	4.1	14
160	0.42	1.3	1.5	3.8	0.21	0.57	4.1	14
170	0.42	1.3	1.5	3.7	0.20	0.56	4.0	13
180	0.42	1.3	1.4	3.7	0.20	0.56	3.9	13
190	0.41	1.3	1.4	3.7	0.20	0.55	3.9	13
200	0.40	1.2	1.4	3.6	0.20	0.54	3.8	13

The total ionization cross-section for the production of the parent ion and all 15 fragment ions is also included.

reaction with C_5H_5N, as described in the experimental section. The following reactions are observed, with the branching ratios shown in parentheses:

$$C_5H_5N^+ + C_5H_5N \rightarrow C_5H_6N^+ + C_5H_4N \quad (100\%) \qquad (1)$$

$$C_4H_4^+ + C_5H_5N \rightarrow C_9H_8N^+ + H \quad (54\%) \qquad (2)$$

$$C_4H_4^+ + C_5H_5N \rightarrow C_5H_6N^+ + C_4H_3 \quad (34\%) \qquad (3)$$

$$C_4H_4^+ + C_5H_5N \rightarrow C_5H_5N^+ + C_4H_4 \quad (12\%) \qquad (4)$$

$$C_4H_3^+ + C_5H_5N \rightarrow C_5H_6N^+ + C_4H_2 \quad (99\%) \qquad (5)$$

$$C_4H_3^+ + C_5H_5N \rightarrow C_5H_5N^+ + C_4H_3 \quad (1\%) \qquad (6)$$

$$C_4H_2^+ + C_5H_5N \rightarrow C_5H_5N^+ + C_4H_2 \quad (74\%) \qquad (7)$$

$$C_4H_2^+ + C_5H_5N \rightarrow C_5H_6N^+ + C_4H \quad (26\%) \qquad (8)$$

The formulas for the neutral products in the above equations are derived from our understanding of the reaction mechanisms: reactions (4), (6) and (7) are charge transfer reactions; reactions

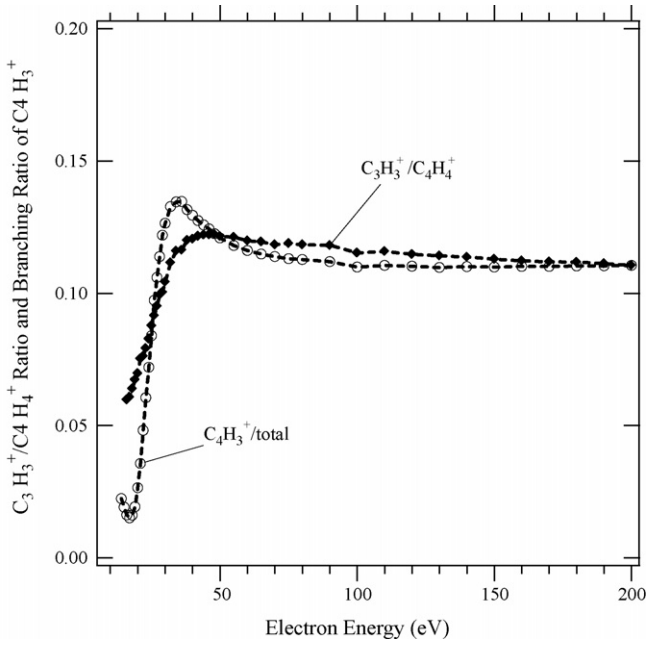

Fig. 3. Ratio of the $C_3H_3^+$ to $C_4H_4^+$ intensities, and the branching ratio of $C_4H_3^+$, as functions of the electron energy.

(1), (3), (5), and (8) are likely to proceeds through a proton transfer mechanism, which is suggested by the observation of the common product ion $C_5H_6N^+$ from all of the four reactant ions. Reaction (2) is assumed to be a condensation followed by H atom elimination. If not thermalized, the protonated pyridine ion, $C_5H_6N^+$, undergoes further reaction with pyridine to form $C_9H_8N^+$; if thermalized by collisions with Ar gas before it collides with pyridine, no reaction is observed. The product ion $C_9H_8N^+$ is found to be unreactive with pyridine. Lifshitz et al. [5] have reported the reaction rates of $C_5H_5N^+$, $C_4H_4^+$ and $C_4H_3^+$, and reported the product ions from $C_4H_4^+$ including the proton transfer product $C_5H_6N^+$ and the condensation product $C_9H_8N^+$; however, the branching ratios were not reported. One difference is our observation of the $C_5H_5N^+$ ion in the $C_4H_4^+$ reaction products formed by charge transfer, which they did not report. We have measured the relative reaction rate coefficients, which are then calibrated against Lifshitz et al.'s reaction rate coefficient for $C_4H_4^+$. The results are shown in Table 2 along with the literature values. In general, as the reactant ion becomes smaller, the reaction rate increases. Also included in Table 2 are the collision rate coefficients calculated from Langevin theory, using 9.5×10^{-24} cm^3 for the polarizability of pyridine [28], and the reaction efficiencies defined as the ratios of the observed reaction rates over the calculated collision rates. It is not clear at this point why the reaction efficiencies for the three smaller ions in Table 2 are greater than unity. It may simply be the result of uncertainties in the measured rates and/or the measured pyridine polarizability, or may indicate an inadequacy of the Langevin formula. Given reasonable uncertainties in the measured quantities and the generally accepted validity of the Langevin rate, it most likely indicates that these reactions are very effective.

$C_4H_4^+$ generated from electron impact ionization of pyridine as well as benzene, etc., is considered to consist of two isomers, vinylacetylene and methylene cyclopropene [4,7,9], which have been found to have different reactivities towards benzene or acetylene: one isomer reacts readily while the other one is essentially unreactive [4,7]. In a study by Shay et al. [29] four different isomers of $C_4H_4^+$ were found to be formed from different neutral precursors, namely, vinylacetylene, butatriene, methylene cyclopropene, and nonaromeatic cyclobutadiene, which undergo significantly different ion-molecule reactions with allene, isoprene, furan, and thiophene. In our study, when $C_4H_4^+$ generated from pyridine reacts with its parent molecule, no evidence of biexponential decay of thermalized $C_4H_4^+$ has been observed. The $C_4H_4^+$ reaction exhibits single exponential behavior until the end of the reaction time at which only ~0.5% of the original population of $C_4H_4^+$ is left. One possible explanation is that the reaction mechanism for $C_4H_4^+$ + pyridine does not significantly differentiate among these isomers; they react with similar rates. To probe the reaction mechanism, specifically for that forming the condensation product ion $C_9H_8N^+$, we have performed a preliminary isotopic reaction study in which a mixture of pyridine and pyridine-d_5 (in a ratio of 2:1) was used. When $C_4D_4^+$ formed by electron impact of C_5D_5N reacts with the mixture, several product ions are detected as shown in Fig. 4, where peaks labeled by formulas are the products identified using the reaction equations mentioned above, namely, condensation reaction (2), proton transfer reaction (3) and charge transfer reaction (4):

$$C_4D_4^+ + C_5H_5N \rightarrow C_9H_5D_3N^+ + D \quad (2a)$$

$$C_4D_4^+ + C_5H_5N \rightarrow C_9H_4D_4N^+ + H \quad (2b)$$

$$C_4D_4^+ + C_5H_5N \rightarrow C_5H_5DN^+ + C_4D_3 \quad (3a)$$

$$C_4D_4^+ + C_5H_5N \rightarrow C_5H_5N^+ + C_4D_4 \quad (4a)$$

Table 2
Ion-molecule reaction rate coefficients from the literature (k_{lit}) and from the current FTMS study (k_{ftms}) (the relative rate coefficients determined in this work are calibrated against the literature value[a] for the $C_4H_4^+$ reaction)

Reaction	k_{lit} ($\times 10^{-10}$ cm^3/s)	k_{ftms} ($\times 10^{-10}$ cm^3/s)	k_{calc} ($\times 10^{-10}$ cm^3/s)	k_{ftms}/k_{calc}
$C_5H_5N^+$ + pyridine	9.8[a]	8.9	11.5	0.77
$C_4H_4^+$ + pyridine	14.6[a], 22[b]	14.6[c]	12.9	1.13
$C_4H_3^+$ + pyridine	18.3[a]	15.5	13.0	1.19
$C_4H_2^+$ + pyridine		16.8	13.0	1.29

Calculated collision rate coefficients (k_{calc}) and the reaction efficiencies (k_{ftms}/k_{calc}) are also included.
[a] Ref. [5].
[b] Ref. [4].
[c] Calibration point.

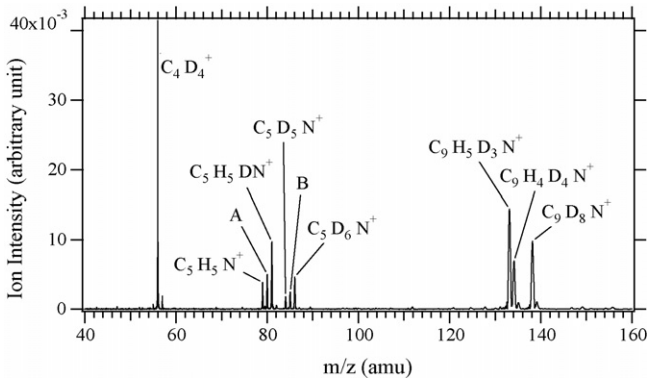

Fig. 4. Mass spectrum of reaction of $C_4D_4^+$ with a mixture of C_5H_5N/C_5D_5N in a ratio of 2:1.

$$C_4D_4^+ + C_5D_5N \rightarrow C_9D_8N^+ + D \quad (2c)$$

$$C_4D_4^+ + C_5D_5N \rightarrow C_5D_6N^+ + C_4D_3 \quad (3b)$$

$$C_4D_4^+ + C_5D_5N \rightarrow C_5D_5N^+ + C_4D_4 \quad (4b)$$

Two peaks in Fig. 4 labeled by "A" and "B" are identified to be $C_5H_6N^+$ and $C_5HD_5N^+$, respectively. These cannot be the direct products of $C_4D_4^+ + C_5H_5N$, because the atom number cannot be balanced, and therefore are assumed to be from the secondary reaction of $C_5H_5N^+$ that is the product ion of (4a) and (4b):

$$C_5H_5N^+ + C_5H_5N \rightarrow C_5H_6N^+ + C_5H_4N \quad (1a)$$

$$C_5H_5N^+ + C_5D_5N \rightarrow C_5HD_5N^+ + C_5H_4N. \quad (1b)$$

It is also possible that the product ion in (3a), protonated pyridine C_5H_5N–D^+, undergoes H atom scrambling to form C_5H_4DN–H^+ that in turn undergoes symmetric proton transfer with C_5H_5N:C_5D_5N:

$$C_5H_4DN\text{–}H^+ + C_5H_5N \rightarrow C_5H_5N\text{–}H^+ + C_5H_4DN$$

$$C_5H_4DN\text{–}H^+ + C_5D_5N \rightarrow C_5D_5N\text{–}H^+ + C_5H_4DN$$

In Fig. 4 one can see the branching ratio of (2a) versus (2b) is ~2:1, indicating the apparent preference of D atom loss over H atom loss from the condensation product. In other words, the mechanism of the condensation reaction of $C_4H_4^+$ with pyridine favors the loss of an H atom originally from the ionic reactant over an H atom originally from the neutral reactant by a factor of ~2. A systematic study involving theoretical calculations and experiments using substituted pyridine is underway.

4. Summary

Electron impact ionization of pyridine produces the parent ion and 15 fragment ions having cross-sections grater than 10^{-18} cm^2 at 30 eV. The parent ion $C_5H_5N^+$ and fragment ion $C_4H_4^+$ are the most abundant ions throughout the energy range of 10–200 eV, contributing 55% or more of the total ion population. The total cross-section reaches a maximum of 1.5×10^{-15} cm^2 at ~90 eV. The neutral product output of the total electron impact ionization is believed to be dominated by H atoms and HCN molecules formed through the major dissociation channels. The reactions of four important ions, $C_5H_5N^+$, $C_4H_4^+$, $C_4H_3^+$, and $C_4H_2^+$, with their parent molecule, are found to share a commonality in that they all proceed through the charge transfer or proton transfer mechanisms, with $C_4H_4^+$ undergoing condensation followed by H elimination in addition. The final product ion is the protonated pyridine ion, $C_5H_6N^+$, which is formed with sufficient internal energy so that part of its population is found to further react with pyridine forming $C_9H_8N^+$. $C_9H_8N^+$ is unreactive with pyridine. The reaction rate coefficients for the four reactant ions are found to increase as the mass of the reactant ion decreases.

Acknowledgements

The authors thank the Air Force Office of Scientific Research for support. We also thank Dr. Huo for alerting us to the need for low energy electron impact absolute cross-sections for pyridine.

References

[1] R.J. Dickinson, D.H. Williams, J. Chem. Soc. Perkin Trans. 2 (1972) 1363.
[2] H. Ichikawa, M. Ogata, J. Am. Chem. Soc. 95 (1973) 806.
[3] H.M. Rosenstock, K.E. McCullogh, F.P. Lossing, Int. J. Mass Spectrom. Ion Phys. 25 (1977) 327.
[4] P. Ausloos, J. Am. Chem. Soc. 103 (1981) 3931.
[5] C. Lifshitz, D. Gibson, K. Levsen, I. Dotan, Int. J. Mass Spectrom. Ion Phys. 40 (1981) 157.
[6] C. Lifshitz, J. Phys. Chem. 86 (1982) 606.
[7] W. Wagner-Redeker, A.J. Illies, P.R. Kemper, M.T. Bowers, J. Am. Chem. Soc. 105 (1983) 5719.
[8] P.C. Burgers, J.L. Holmes, Int. J. Mass Spectrom. Ion Process 58 (1984) 15.
[9] R. Arakawa, M. Arimura, Y. Yoshidawa, Int. J. Mass Spectrom. Ion Process 64 (1985) 227.
[10] R. Arakawa, Y. Yoshikawa, Bull. Chem. Soc. Jpn. 60 (1987) 49.
[11] E. Gridelet, R. Locht, A.J. Lorquet, J.C. Lorquet, B. Leyh, Int. J. Mass Spectrom. 228 (2003) 389.
[12] (a) C. Dateo, W. Huo, Bull. Am. Phys. Soc. 47 (2002) 12;
(b) W.M. Huo, Phys. Rev. A 64 (2001) 042719.
[13] P.D. Haaland, Chem. Phys. Lett. 170 (1990) 146.
[14] M.B. Comisarow, A.G. Marshall, Chem. Phys. Lett. 25 (1974) 282.
[15] A.G. Marshall, P.B. Grosshans, Anal. Chem. 63 (1991) 215A.
[16] Z. Liang, A.G. Marshall, Anal. Chem. 62 (1990) 70.
[17] A.G. Marshall, T.L. Wang, T.L. Ricca, J. Am. Chem. Soc. 107 (1985) 7983.
[18] S. Guan, Chem. Phys. 91 (1989) 775.
[19] L. Chen, A.G. Marshall, Int. J. Mass Spectrom. Ion Process 79 (1987) 115.
[20] D.L. Rempel, S.K. Huang, M.L. Gross, Int. J. Mass Spectrom. Ion Process 70 (1986) 163.
[21] H.C. Straub, P. Renault, B.G. Lindsay, K.A. Smith, R.F. Stebbings, Phys. Rev. A 52 (1995) 1115.
[22] R.C. Wetzel, F.A. Baiocchi, T.R. Hayes, R.S. Freund, Phys. Rev. A 35 (1987) 559.
[23] S. Guan, A.G. Marshall, Int. J. Mass Spectrom. Ion Process 146/147 (1995) 261.
[24] M. Wang, A.G. Marshall, Anal. Chem. 61 (1989) 1288.
[25] ELG-2A Electron Gun Instruction Manual, Kimball Physics Inc., Wilton, New Hampshire, 1986.
[26] T. Baer, G.D. Willett, D. Smith, J.S. Phillips, J. Chem. Phys. 70 (1979) 4076.

[27] For more information on the branching ratio of the competing unimolecular reactions in terms of the RRKM-QET theory, see:
D.H. Williams, I. Howe, Principles of Organic Mass Spectrometry, McGraw-Hill, London, 1972.
[28] D.R. Lide (Ed.), CRC Handbook of Chemistry and Physics, 81st ed., CRC Press, Washington, DC, 2000.
[29] B.J. Shay, M.N. Eberlin, R.G. Cooks, J. Am. Soc. Mass Spectrom. 3 (1992) 518.